Electronic and Vibrational States of Single Tin−Phthalocyanine Molecules in Double Layers on Ag(111)

F. Schwarz,*,† Y. F. Wang,‡ W. A. Hofer,§ R. Berndt,∥ E. Runge,† and J. Kröger*,†

†Institut für Physik, Technische Universität Ilmenau, D-98693 Ilmenau, Germany
‡Key Laboratory for the Physics and Chemistry of Nanodevices, Department of Electronics, Peking University, Beijing 100871, China
§School of Chemistry, Newcastle University, Newcastle NE1 7RU, United Kingdom
∥Institut für Experimentelle und Angewandte Physik, Christian-Albrechts-Universität zu Kiel, D-24098 Kiel, Germany

ABSTRACT: Electronic and vibrational properties of the two stable molecular configurations of Sn−phthalocyanine adsorbed on an ultrathin Sn−phthalocyanine buffer film on Ag(111) have been investigated with scanning tunneling microscopy and density functional calculations. Complex submolecular patterns are experimentally observed in unoccupied states images. The calculations show that they result from a superposition of Sn p orbitals. Furthermore, the characteristic features in spectra of the differential conductance are reproduced by the calculations together with a remarkable difference between the two configurations. First-principles calculations show that rather than a single vibrational mode and its higher harmonics the excitations of different molecular vibrational quanta induce replica of orbital spectroscopic signatures. The replicated orbital features appear for the configuration with a low molecule−surface coupling. To model spectra of molecules with a larger coupling to the surface it is sufficient to consider elastic tunneling to orbital resonances alone.
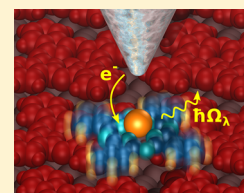
INTRODUCTION

Local injection of electrons and holes from the tip of a scanning tunneling microscope (STM) may be used to explore the electronic and vibrational properties of single molecules with submolecular precision. Electronic excitations may readily be probed by elastic tunneling of electrons from occupied and to unoccupied molecular resonances. Inelastic tunneling processes involve the excitation of photon emission,[1] vibrations,[2] and spin flips.[3] Since the first observation of single-molecule vibrational modes,[2] vibrational spectroscopy with the STM has been reported for a variety of molecules, as summarized in pertinent review articles.[4−8] To enhance the coupling between the injected electron and molecular vibrational degrees of freedom, buffer layers[9−16] and suitably designed molecular platforms[17−19] have been used. In such experiments fingerprints of a single vibrational mode and its higher harmonics were reported as satellite peaks to the spectroscopic signature of a molecular orbital.[10,11,18]

The modeling of spectra of the differential conductance (dI/dV) of molecules with a large number of atoms and a low symmetry of the adsorption complex remains a challenge to state-of-the-art calculations. Approaches based on *ab initio* calculations for many-electron systems have been developed.[20−24] They were successfully applied to simple molecules[20,21,23,25−27] and molecules with high symmetry.[17,28−30] However, complex molecules play an important role for molecular electronics: they often provide bistable configurations that may be interconverted by electron and hole injection. Therefore, the description of electronic and vibrational properties of complex molecules is highly desirable.

In this work STM images and dI/dV spectra are calculated and compared to experimental data from two configurations of

tin−phthalocyanine (Sn−$C_{32}N_8H_{16}$, SnPc) adsorbed on a single SnPc buffer layer on Ag(111). The two configurations are characterized by the central Sn atom pointing toward vacuum (SnPc↑) and toward the surface (SnPc↓). STM images of both configurations exhibit complex submolecular patterns, which are reproduced by the simulations. In particular, unlike STM images of all phthalocyanine and porphyrin molecules with a metal center reported to date the central Sn atom of SnPc↑ appears as a central protrusion with internal structure. The calculations trace this observation to the intersection of nodal planes of Sn p_x and Sn p_y orbitals. Moreover, dI/dV spectra of SnPc↑ exhibit vibronic excitations. Their energies being comparable to those of electronic transitions call for going beyond the quasistatic approximation in calculating inelastic and elastic tunneling from first-principles. We find that spectroscopic replicas of molecular orbitals are due to a combination of vibrational modes rather than a single one and its harmonics. In contrast, spectra of SnPc↓ are modeled by solely taking elastic tunneling into molecular orbitals into account. We hint that the different degrees of hybridization with the substrate are the origin to the different levels of modeling.

EXPERIMENT

Experiments were performed with a STM operated at 7 K and in ultrahigh vacuum (10^{-9} Pa). Ag(111) surfaces were cleaned by Ar+ bombardment and subsequent annealing. SnPc molecules were sublimated from a heated Ta crucible and

deposited on Ag(111) at room temperature. All STM images were acquired in the constant-current mode with the voltage applied to the sample. Constant-height spectra of dI/dV were obtained by modulating the sample voltage (10 mV$_{rms}$, 900 Hz) and measuring the current response of the tunneling junction with a lock-in amplifier.

RESULTS AND DISCUSSION

Figures 1a and 1b show constant-current STM images of a single SnPc↑ and a single SnPc↓, respectively, adsorbed on top
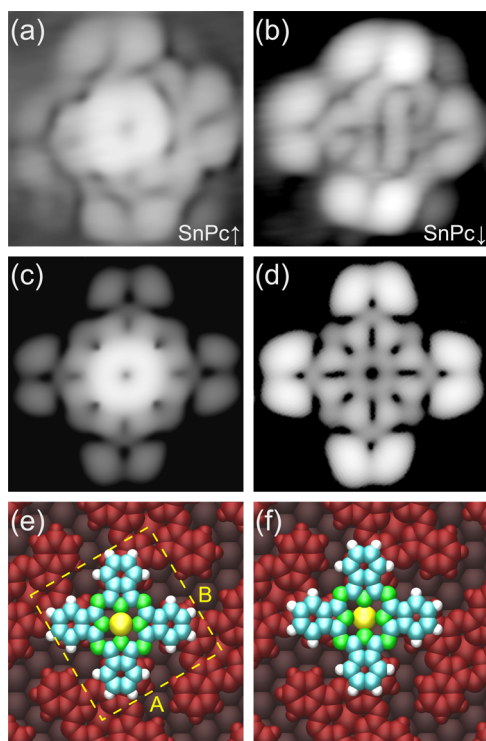

Figure 1. (a, b) Experimental constant-current STM images of SnPc↑ (a) and SnPc↓ (b) adsorbed on top of a SnPc buffer layer on Ag(111) (0.9 V, 60 pA, 2 × 2 nm^2). The apparent heights range from 0 pm (black) to 300 pm (white) for SnPc↑ and to 240 pm (white) for SnPc↓. (c, d) Calculated constant-current STM images of SnPc↑ (c) and SnPc↓ (d) adsorbed on a SnPc↓ buffer layer on Ag(111) (1.8 × 1.8 nm^2). The bias voltage was set to 0.22 V (SnPc↑) and 0.24 eV (SnPc↓) and the tip–surface distance to 350 pm. The grayscale ranges from 0 pm (black) to 230 pm (white) for SnPc↑ and to 130 pm (white) for SnPc↓. (e, f) Sketches of unit cells used in the calculations for SnPc↑ (e) and SnPc↓ (f). The buffer layer consists of SnPc↓ molecules (red) whose central Sn atom resides on hexagonal close-packed sites of the Ag(111) lattice (brown).

of a single SnPc layer on Ag(111). The first molecular layer is closed, and SnPc molecules in this layer predominantly adopt the ↓ configuration.[31] The STM image of the Sn atom of SnPc↑ is remarkable. It exhibits a ≈230 pm protrusion on top of which we observe a shallow depression. This is different from the STM images of all other metal ions in phthalocyanines reported so far, which exhibit either a protrusion or a depression but lack further internal structure.[32−44] The occurrence of the metal center as a protrusion or a depression in STM images has been demonstrated to depend on the density of metal d states at the Fermi energy (E_F).[34] Below we will show that for SnPc the Sn p orbitals are most relevant to empty-states STM images.

Constant-current empty-states STM images were calculated (Figures 1c,d) to determine the origin of the peculiar appearance of the central region of SnPc↑ and to identify the molecular orbitals that contribute to the STM images. To this end, density functional calculations were performed with the Vienna *ab initio* simulation package (VASP)[45−48] for a two-layer Ag slab. The projector-augmented wave pseudopotential with the parametrization of Perdrew, Burke, and Ernzerhof[49,50] was used with a plane-wave cutoff set to 400 eV. Only the Γ point of the Brillouin zone ($k = 0$) needs to be considered due to flat bands in the energy region of interest. Experimental STM images served as an initial estimate for the determination of the favored adsorption site. In particular, for the first molecule layer a rectangular unit cell of SnPc↓ molecules with dimensions A = 1.470 nm and B = 1.528 nm (dashed lines in Figure 1e) was assumed, which approximates the unit cell reported in previous works.[31,51−53] The structural optimization positioned the SnPc molecules of the second layer with their isoindole groups atop the isoindole groups of first-layer molecules (Figures 1e,f). This stacking results in an angle of 30° enclosed by isoindole directions of the first and second layer. Interactions between the two SnPc layers are dominated by van der Waals forces. Thus, the exact position of the adsorbed molecule has little influence on electronic and vibrational properties. Grimme-type corrections to the correlation functional were then used to take van der Waals interactions into account and for further structure optimization. In the relaxed geometry all forces were lower than 150 meV nm^{-1}. For the relaxed molecules constant-current STM images and dI/dV spectra were calculated with the Tersoff−Hamann model[54,55] using bSKAN.[56−58]

The calculations show that SnPc molecules adsorbed within the buffer layer adopt the ↓ configuration with the central Sn residing atop hexagonal close-packed Ag(111) sites.[59] The calculated adsorption energy (−5.264 eV) is mainly due to van der Waals interaction and ≈0.1 eV lower than adsorption energies obtained for on-top, bridge, and face-centered cubic Ag(111) sites. The bias voltage in the calculations has been set to 0.22 V (SnPc↑) and 0.24 V (SnPc↓), which enables tunneling into the group of four lowest unoccupied molecular orbitals (LUMOs), whose energies were calculated as 0.14, 0.16, 0.2, and 0.22 eV (SnPc↑) and 0.13, 0.15, 0.195, and 0.235 eV (SnPc↓). For SnPc↑, the LUMOs at 0.2 and 0.22 eV dominate the vacuum density of states. While simulated and experimental STM images are in good agreement, the bias voltages used in the calculations and in the experiments deviate from each other. We attribute this discrepancy to the well-known difficulty in defining the Fermi energy in density functional calculations of adsorbates. Cross-sectional profiles of SnPc↑ across the molecular center are shown by the top green (experimental) and the bottom red (calculated) line in Figure 2a. The calculated data (lower line in Figure 2a) represent the solution of the Tersoff−Hamann model with no additional numerical broadening. These data were divided by a factor 2 to facilitate the comparison with experimentally obtained apparent heights. Importantly, the main unexpected feature, namely the depression in the central protrusion, is reproduced by the calculation. Since the simulations enable a decomposition of the calculated local density of states into the contributions of individual orbitals, we could trace the peculiar appearance of the molecule center to p_x and p_y orbitals of Sn. These orbitals dominate the SnPc↑ LUMOs and exhibit an appreciable vacuum density of states in the relevant energy range. The Sn
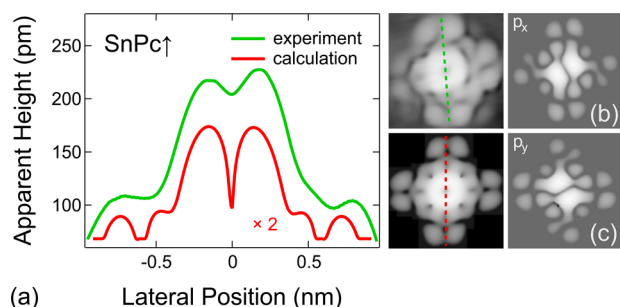
Figure 2. (a) Experimental (top green line) and calculated (bottom red line) cross-sectional profiles across SnPc↑ along the dashed lines indicated in the panels on the right, which show an experimental (top, same as Figure 1a) and calculated (bottom, same as Figure 1c) STM image of SnPc↑. The Sn atom is centered at 0 nm. The calculated data (lower line) represent the solution of the Tersoff–Hamann model without additional numerical broadening. The central depression within the Sn-related protrusion is clearly visible in both data sets. (b, c) Spatial distribution of the squared amplitude of Kohn–Sham states that dominate the low-bias tunneling. These states show the symmetry of Sn p_x and Sn p_y orbitals. The amplitude was evaluated in the vacuum region 350 pm above the molecule.

p_x and Sn p_y orbitals interact with linear combinations of Pc orbitals that exhibit the same symmetry. This hybridization leads to two pairs of LUMOs with approximate p_x and p_y symmetry and similar energies. The spatial distribution of the squared amplitude of the relevant Kohn–Sham states is depicted in Figures 2b,c. The other two states with similar energy (not shown) show a similar lateral density pattern but decay much faster in the vacuum and, thus, do not contribute significantly to the simulated STM images. Both p_x and p_y orbitals are characterized by a nodal plane across the molecule center. Any combination of these orbitals results in a central depression of the local density of states, which is located at the intersection of the nodal planes. Unlike the p_x and p_y orbitals the Sn p_z orbital does not participate significantly in the hybridization with Pc orbitals. Therefore, the Sn p_z energy is more than 1 eV higher than the p_x and p_y energies, and the contribution of the p_z orbital to the total local density of states is negligibly small at the relevant energies. These findings may hold as well for other central atoms with partially filled p shells, such as Pb.

Next we present dI/dV spectra of unoccupied states acquired with the tip atop the centers of SnPc↑ (Figure 3a) and SnPc↓ (Figure 3b). Both spectra exhibit several peaks, which are labeled $\alpha_\uparrow$, $\beta_\uparrow$, and $\gamma_\uparrow$ ($\alpha_\downarrow$, $\beta_\downarrow$, $\gamma_\downarrow$, and $\delta_\downarrow$) and whose energies are summarized in Table 1.[60,61] Since spectra of dI/dV are featureless for molecules adsorbed to Ag(111),[31] we conclude that indeed the single SnPc layer efficiently reduces the hybridization of second-layer molecules with the metal substrate. To identify the experimentally observed spectroscopic features, spectra of dI/dV were simulated. Figures 3c,d show calculated spectra for which solely elastic tunneling into empty molecular resonances was considered. In the calculations the tip was placed 450 pm above the molecular center, and the calculated current was averaged over a circular area with a diameter of 100 pm (red dots in the insets to Figures 3c,d). The first peak consists of four nearly degenerate Sn p resonances whose energies are indicated by the vertical lines at the bottom of the plots. For SnPc↑ (Figure 3c) the two low-energy resonances are visible as a shoulder to the main LUMO feature. Apart from this dominant contribution to the calculated
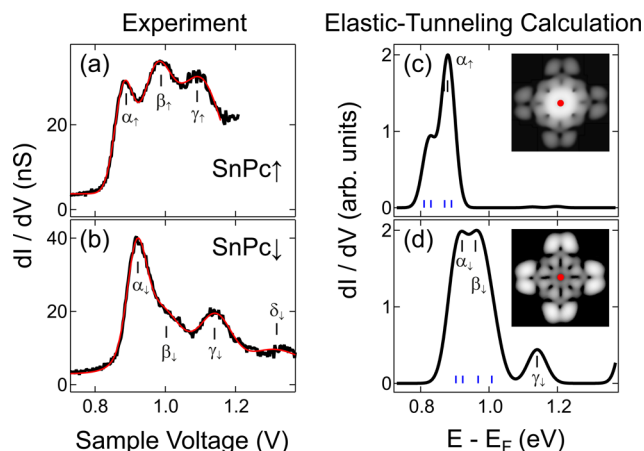
Figure 3. (a, b) Constant-height spectra of dI/dV acquired atop the center of (a) SnPc↑ and (b) SnPc↓ adsorbed on a closed SnPc buffer layer on Ag(111). The feedback loop had been disabled at 1.2 V (SnPc↑) and 1.5 V (SnPc↓). The full lines show fits by a superposition of Gaussians and a linear background. The energies of the Gaussian maxima are summarized in Table 1. (c, d) Calculated dI/dV spectra taking solely elastic current contributions into account. The tip–molecule distance was set to 450 pm. The spectra were horizontally shifted until the calculated LUMO peak matched the experimentally observed peak $\alpha_\uparrow$ ($\alpha_\downarrow$). Vertical lines at the bottom of the panels mark calculated LUMO energies. The calculated spectrum was broadened by a convolution with a Gaussian [full width at half-maximum 42 meV (SnPc↑) and 64 meV (SnPc↓)]. The insets to (c) and (d) show calculated STM images of SnPc↑ and SnPc↓, respectively. The central red dots indicate the positions and the averaging areas (diameter: 100 pm) of calculated dI/dV data.

dI/dV data the simulated data are rather featureless. Only weak peaks are visible at higher energies. The experimentally observed peaks $\beta_\uparrow$ and $\gamma_\uparrow$ (Figure 3a) are absent from the calculated spectrum. Obviously, elastic contributions alone fail to reproduce experimental data. Below we show that adding inelastic electron tunneling processes improves the comparison considerably.

The situation is different for SnPc↓. While the calculated peak height ratios do not exactly match the experimental observations, the calculated elastic tunneling spectra (Figure 3d) reproduce the main experimental features $\alpha_\downarrow$, $\beta_\downarrow$, and $\gamma_\downarrow$. Features $\alpha_\downarrow$ and $\beta_\downarrow$ comprise contributions of Sn p orbitals. These p orbitals are likewise present in the SnPc↑ case. For SnPc↓ the energies of these resonance cover a wider range, which is likely due to an increased level splitting caused by the Sn ion hybridizing with molecules of the buffer layer and the Ag(111) surface. The peak labeled $\gamma_\downarrow$ corresponds to an orbital with a laterally uniform density and a low vacuum amplitude. It appears prominently in the spectra since in the center of the molecule the density of states of all other orbitals is low. We suggest that this feature originates from the buffer layer or the substrate.

Before considering inelastic contributions to the spectra, we comment on the assignment of the LUMO to features $\alpha_\uparrow$ and $\alpha_\downarrow$. Two findings lend support to this assignment. First, simulated STM images at the bias voltage corresponding to the calculated LUMO energy are in accordance with experimental data (Figures 1a—d). Second, the calculated energy of the highest occupied molecular orbital (HOMO) is −1.6 eV for SnPc↑ and −1.7 eV for SnPc↓, giving rise to a HOMO−LUMO

Table 1. Experimental and Calculated Energies (eV) of Spectroscopic Features $\alpha_\uparrow$, $\beta_\uparrow$, and $\gamma_\uparrow$ ($\alpha_\downarrow$, $\beta_\downarrow$, $\gamma_\downarrow$, and $\delta_\downarrow$)^a

configuration	$\alpha_{\uparrow,\downarrow}$	$\beta_{\uparrow,\downarrow}$	$\gamma_{\uparrow,\downarrow}$	$\delta_\downarrow$	
SnPc↑	0.88 ± 0.01	0.98 ± 0.02	1.10 ± 0.02		experiment
	0.88				calculation (elastic)
	0.88	0.93	1.04		calculation (inelastic)
SnPc↓	0.92 ± 0.01	1.01 ± 0.04	1.15 ± 0.02	1.35 ± 0.04	experiment
	0.92	0.97	1.14		calculation (elastic)

^{a}Maxima in experimental spectra were determined from Gaussian fits to the data (Figures 3a,b). The calculated energy of feature $\alpha_\uparrow$ ($\alpha_\downarrow$) was set to the experimental value (see text). In the calculations elastic and inelastic (eq 1) contributions to the dI/dV spectra were considered.

gap of ≈ 1.9 eV, which matches well the experimentally observed gap of ≈ 2.1 eV.[31]

To describe the experimental dI/dV spectra of SnPc↑ adequately, vibrational excitations of the molecule have to be taken into account.[62] In previous publications several features were observed within the spectroscopic signature of a molecular orbital[10,11,19] and attributed to a single vibrational state and its higher harmonics. For our sample molecular vibrations have been calculated in the energy range of 15 meV $\leq \hbar\Omega \leq$ 390 meV. Describing vibrational excitations with lower energies such as frustrated translations and rotations is difficult with the employed simulation methods.[63] Therefore, we restricted our calculations to the aforementioned energy range. The contributions of vibrations to the tunneling current were evaluated in lowest-order perturbation theory according to a previous approach.[64,65] Thus, multiple emission of vibrational quanta is not included. We will show below that overtones of a vibrational mode are not needed to explain experimental data. The code of Teobaldi et al.[65] was modified in order to be able to go beyond the quasistatic approximation. This approximation assumes $\hbar\Omega \ll |E_\mu - E_\nu|$ (E_μ, E_ν: energies of molecular electronic states) and sets $\Omega \equiv 0$ in eqs 1 and 2. This modification is important since vibrational energies and differences between molecular orbitals are of comparable magnitude in the present case. The dI/dV spectrum at bias voltage V and tip position $\mathbf{r}_0$ reads including elastic (first term, dI_0/dV) and inelastic (second term, dI_{vib}/dV) contributions

$$\left.\frac{dI}{dV}\right|_{V,\mathbf{r}_0} = \left.\frac{dI_0}{dV}\right|_{V,\mathbf{r}_0} + \left.\frac{dI_{vib}}{dV}\right|_{V,\mathbf{r}_0}$$

$$= \sum_\mu |\langle \mathbf{r}_0 | \Psi_\mu \rangle|^2 \delta(E_\mu - E_F - eV)$$

$$+ \sum_{\mu,\lambda} |\langle \mathbf{r}_0 | \delta\Psi_\mu^\lambda \rangle|^2 \delta(E_\mu + \hbar\Omega_\lambda - E_F - eV) \quad (1)$$

where Ψ_μ is the μth eigenstate of the sample, E_μ its energy eigenvalue, and $\hbar\Omega_\lambda$ the energy of vibration λ. The change of Ψ_μ due to the vibration mode λ, $\delta\Psi_\mu^\lambda$, is evaluated in lowest-order perturbation theory as

$$|\delta\Psi_\mu^\lambda\rangle = \sum_\nu |\Psi_\nu\rangle \frac{V_{\nu\mu}^\lambda}{E_\mu + \hbar\Omega_\lambda - E_\nu + i\eta} \quad (\eta \to 0) \quad (2)$$

with the matrix element of the deformation potential $V_{\mu\nu}^\lambda$ being calculated with a finite-differences approach.[65] For the actual calculations, we restricted the sum over all vibrational modes λ to the vibrations involving the topmost SnPc molecule since the expression for the inelastic tunneling contribution involves the wave function values at the tip position.

The second delta function in eq 1 shows that vibrations replicate orbital-related signatures at $E_\mu + \hbar\Omega_\lambda$. In this case the

electron with energy eV tunnels into the molecular resonance with energy E_μ by emitting a vibrational quantum with energy $\hbar\Omega_\lambda$,[66] giving rise to a spectroscopic feature at $E_F + eV = E_\mu + \hbar\Omega_\lambda$. For highly symmetric molecules group theory can be used to prove that certain $V_{\mu\nu}^\lambda$ vanish.[67] In the present case, however, the interaction of SnPc with adjacent molecules of the buffer layer and with Ag(111) likely lifts all symmetries and leads to nonzero, albeit possibly small, $V_{\mu\nu}^\lambda$. The calculated dI/dV spectrum of SnPc↑ with vibration corrections is displayed in Figure 4. In agreement with the experiment (Figure 3a) three
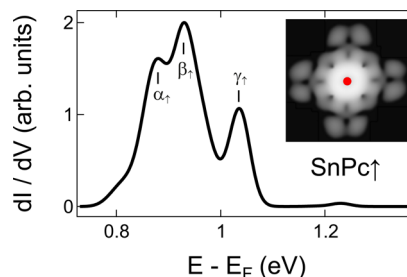
Figure 4. Calculated dI/dV spectrum for SnPc↑ including first-order corrections from inelastic vibration excitations (eq 1). The spectra were horizontally shifted until experimental and calculated $\alpha_\uparrow$ peaks coincided.

peaks are present. The calculated peak energies are in accordance with the experimental values (Table 1).[60,61] Each peak comprises several vibrational modes and cannot be attributed to a single mode. Vibration modes that strongly contribute to $\alpha_\uparrow$ are characterized by an in-plane displacement of the central Sn atom. Peak $\beta_\uparrow$ is mainly induced by C and N out-of-plane bending modes, while feature $\gamma_\uparrow$ originates from C—C and C—N in-plane stretching vibrations. As a result, adding inelastic electron tunneling contributions to the elastic tunneling current leads to an improved agreement between the calculated dI/dV data and the experimental data for SnPc↑ (Figure 3a).

The situation is quite different for SnPc↓, where experimental data are semiquantitatively described by the elastic tunneling current alone. Because of the larger energy differences of the low-energy unoccupied molecular orbitals (*vide supra*), the elastic spectrum already shows several peaks in the range of vibrational energies (Figure 3d). In this case, replica of molecular orbitals with energy E_μ coincide with orbitals at E_ν, where $E_\mu - E_\nu = \hbar\Omega_\lambda$. Therefore, replica peaks do not lead to additional features in dI/dV spectra. According to eq 2, the situation $E_\mu - E_\nu = \hbar\Omega_\lambda$ is not adequately described by the perturbation approach. The vanishing denominator leads to unrealistically high dI_{vib}/dV values for nonzero $V_{\nu\mu}^\lambda$. A model that takes the polaronic nature of the inelastic excitation process into account (*vide infra*) may more realistically describe

the strength of vibrational lines in dI/dV spectra. The descriptions of SnPc↑ and SnPc↓ dI/dV spectra deviate from each other, which is rationalized in terms of the different molecule−surface coupling arising from the different positions of the central Sn atom.

Going beyond the quasistatic approximation, i.e., $\hbar\Omega_\lambda \neq 0$, exposes a weakness of the perturbation approach. Conceptually, the wave function correction (eq 2) is independent of the bias voltage V. However, inserting the energy conservation $E_\mu + \hbar\Omega_\lambda - E_F - eV = 0$ into eq 2 yields the denominator $E_\nu - E_F - eV - i\eta$. Consequently, the perturbatively evaluated inelastic tunneling current diverges if resonant elastic tunneling (into level Ψ_ν) is possible at nearly the same bias voltage. This divergence reflects the breakdown of the Born−Oppenheimer approximation. In a previous report on oligothiophene molecular wires a non-Born−Oppenheimer regime was suggested.[68] We expect that this intrinsic conceptual weakness may only be overcome in a theory accounting for the polaronic nature of the electronic excitation, which then serves as a basis for degenerate perturbation theory. The quasistatic approximation does not solve this difficulty. Rather, it hides the difficulty by excluding resonant, i.e., vanishing, denominators.

■ CONCLUSIONS

Ab initio calculations have been successful in describing an adsorbed molecule with a high number of different atoms and a low symmetry of the adsorbate complex, SnPc, on a molecular buffer layer on Ag(111). Empty-states STM images of both bistable molecule configurations, SnPc↑ and SnPc↓, are due to the lowest unoccupied molecular orbitals, which are dominated by p orbitals of the central metal ion. Lowest-order perturbation theory showed that the inelastic excitation of molecular vibrational quanta leads to replica of spectroscopic signatures of molecular orbitals. The replicated electronic resonances are due to a combination of vibrational excitations of the molecule, rather than to a single mode and its overtones. Our perturbative approach relies on the Born−Oppenheimer approximation and does not quantitatively account for the strengths of vibrational signals. Future calculations should therefore take the polaronic nature of the inelastic excitation process into account.

■ AUTHOR INFORMATION

Corresponding Authors
*E-mail: felix.schwarz@tu-ilmenau.de (F.S.).
*E-mail: joerg.kroeger@tu-ilmenau.de (J.K.).

Notes
The authors declare no competing financial interest.

■ ACKNOWLEDGMENTS

■ REFERENCES

(1) Berndt, R.; Gaisch, R.; Gimzewski, J. K.; Reihl, B.; Schlittler, R. R.; Schneider, W. D.; Tschudy, M. Photon Emission at Molecular Resolution Induced by a Scanning Tunneling Microscope. *Science* **1993**, *262*, 1425−1427.

(2) Stipe, B. C.; Rezaei, M. A.; Ho, W. Single-Molecule Vibrational Spectroscopy and Microscopy. *Science* **1998**, *280*, 1732−1735.

(3) Heinrich, A. J.; Gupta, J. A.; Lutz, C. P.; Eigler, D. M. Single-Atom Spin-Flip Spectroscopy. *Science* **2004**, *306*, 466−469.

(4) Ho, W. Single-Molecule Chemistry. *J. Chem. Phys.* **2002**, *117*, 11033−11061.

(5) Lorente, N.; Rurali, R.; Tang, H. Single-Molecule Manipulation and Chemistry with the STM. *J. Phys.: Condens. Matter* **2005**, *17*, S1049−S1074.

(6) Hla, S.-W. Scanning Tunneling Microscopy Single Atom/Molecule Manipulation and its Application to Nanoscience and Technology. *J. Vac. Sci. Technol., B* **2005**, *23*, 1351−1360.

(7) Franke, K. J.; Pascual, J. I. Effects of Electron-Vibration Coupling in Transport through Single Molecules. *J. Phys.: Condens. Matter* **2012**, *24*, 394002.

(8) Morgenstern, K.; Lorente, N.; Rieder, K.-H. Controlled Manipulation of Single Atoms and Small Molecules Using the Scanning Tunnelling Microscope. *Phys. Status Solidi B* **2013**, *250*, 1671−1751.

(9) Qiu, X. H.; Nazin, G. V.; Ho, W. Vibrationally Resolved Fluorescence Excited with Submolecular Precision. *Science* **2003**, *299*, 542−546.

(10) Qiu, X. H.; Nazin, G. V.; Ho, W. Vibronic States in Single Molecule Electron Transport. *Phys. Rev. Lett.* **2004**, *92*, 206102.

(11) Wu, S. W.; Nazin, G. V.; Chen, X.; Qiu, X. H.; Ho, W. Control of Relative Tunneling Rates in Single Molecule Bipolar Electron Transport. *Phys. Rev. Lett.* **2004**, *93*, 236802.

(12) Ćavar, E.; Blüm, M.-C.; Pivetta, M.; Patthey, F.; Chergui, M.; Schneider, W.-D. Fluorescence and Phosphorescence from Individual C_{60} Molecules Excited by Local Electron Tunneling. *Phys. Rev. Lett.* **2005**, *95*, 196102.

(13) Repp, J.; Meyer, G.; Paavilainen, S.; Olsson, F. E.; Persson, M.; Persson, M. Scanning Tunneling Spectroscopy of Cl Vacancies in NaCl Films: Strong Electron-Phonon Coupling in Double-Barrier Tunneling Junctions. *Phys. Rev. Lett.* **2005**, *95*, 225503.

(14) Franke, K. J.; Schulze, G.; Henningsen, N.; Fernández-Torrente, I.; Pascual, J. I.; Zarwell, S.; Rück-Braun, K.; Cobian, M.; Lorente, N. Reducing the Molecule-Substrate Coupling in C_{60}-Based Nanostructures by Molecular Interactions. *Phys. Rev. Lett.* **2008**, *100*, 036807.

(15) Wang, Y. F.; Kröger, J.; Berndt, R.; Tang, H. Molecular Nanocrystals on Ultrathin NaCl Films on Au(111). *J. Am. Chem. Soc.* **2010**, *132*, 12546−12547.

(16) Pavliček, N.; Swart, I.; Niedenführ, J.; Meyer, G.; Repp, J. Symmetry Dependence of Vibration-Assisted Tunneling. *Phys. Rev. Lett.* **2013**, *110*, 136101.

(17) Frederiksen, T.; Franke, K. J.; Arnau, A.; Schulze, G.; Pascual, J. I.; Lorente, N. Dynamic Jahn-Teller Effect in Electronic Transport through Single C_{60} Molecules. *Phys. Rev. B* **2008**, *78*, 233401.

(18) Matino, F.; Schull, G.; Köhler, F.; Gabutti, S.; Mayor, M.; Berndt, R. Electronic Decoupling of a Cyclophane from a Metal Surface. *Proc. Natl. Acad. Sci. U. S. A.* **2011**, DOI: 10.1073/pnas.1006661107.

(19) Hauptmann, N.; Hamann, C.; Tang, H.; Berndt, R. Soft-Landing Electrospray Deposition of the Ruthenium Dye N3 on Au(111). *J. Phys. Chem. C* **2013**, *117*, 9734−9738.

(20) Mingo, N.; Makoshi, K. Calculation of the Inelastic Scanning Tunneling Image of Acetylene on Cu(100). *Phys. Rev. Lett.* **2000**, *84*, 3694−3697.

(21) Lorente, N.; Persson, M. Theory of Single Molecule Vibrational Spectroscopy and Microscopy. *Phys. Rev. Lett.* **2000**, *85*, 2997−3000.

(22) Lorente, N.; Persson, M.; Lauhon, L. J.; Ho, W. Symmetry Selection Rules for Vibrationally Inelastic Tunneling. *Phys. Rev. Lett.* **2001**, *86*, 2593−2596.

(23) Frederiksen, T.; Brandbyge, M.; Lorente, N.; Persson, M. Inelastic Scattering and Local Heating in Atomic Gold Wires. *Phys. Rev. Lett.* **2004**, *93*, 256601.

(24) Alducin, M.; Sánchez-Portal, D.; Arnau, A.; Lorente, N. Mixed-Valency Signature in Vibrational Inelastic Electron Tunneling Spectroscopy. *Phys. Rev. Lett.* **2010**, *104*, 136101.

(25) Vitali, L.; Ohmann, R.; Kern, K.; Garcia-Lekue, A.; Frederiksen, T.; Sanchez-Portal, D.; Arnau, A. Surveying Molecular Vibrations during the Formation of Metal-Molecule Nanocontacts. *Nano Lett.* **2010**, *10*, 657−660.

(26) Wegner, D.; Yamachika, R.; Zhang, X.; Wang, Y.; Crommie, M. F.; Lorente, N. Adsorption Site Determination of a Molecular Monolayer via Inelastic Tunneling. *Nano Lett.* **2013**, *13*, 2346−2350.

(27) Okabayashi, N.; Paulsson, M.; Ueba, H.; Konda, Y.; Komeda, T. Inelastic Tunneling Spectroscopy of Alkanethiol Molecules: High-Resolution Spectroscopy and Theoretical Simulations. *Phys. Rev. Lett.* **2010**, *104*, 077801.

(28) Pascual, J. I.; Gómez-Herrero, J.; Sánchez-Portal, D.; Rust, H.-P. Vibrational Spectroscopy on Single C_{60} Molecules: The Role of Molecular Orientation. *J. Chem. Phys.* **2002**, *117*, 9531−9534.

(29) Franke, K. J.; Schulze, G.; Pascual, J. I. Excitation of Jahn-Teller Active Modes during Electron Transport through Single C_{60} Molecules on Metal Surfaces. *J. Phys. Chem. Lett.* **2010**, *1*, 500−504.

(30) Stróżecka, A.; Muthukumar, K.; Larsson, J. A.; Dybek, A.; Dennis, T. J. S.; Mysliveček, J.; Voigtländer, B. Electron-Induced Excitation of Vibrations of Ce Atoms Inside a C_{80} Cage. *Phys. Rev. B* **2011**, *83*, 165414.

(31) Wang, Y. F.; Kröger, J.; Berndt, R.; Hofer, W. Structural and Electronic Properties of Ultrathin Tin-Phthalocyanine Films on Ag(111) at the Single-Molecule Level. *Angew. Chem., Int. Ed.* **2009**, *48*, 1261−1265.

(32) Lippel, P. H.; Wilson, R. J.; Miller, M. D.; Wöll, Ch.; Chiang, S. High-Resolution Imaging of Copper-Phthalocyanine by Scanning-Tunneling Microscopy. *Phys. Rev. Lett.* **1989**, *62*, 171−174.

(33) Möller, R.; Coenen, R.; Esslinger, A.; Koslowski, B. The Topography of Isolated Molecules of Copper-Phthalocyanine Adsorbed on GaAs(110). *J. Vac. Sci. Technol., A* **1990**, *8*, 659−660.

(34) Lu, X.; Hipps, K. W.; Wang, X. D.; Mazur, U. Scanning Tunneling Microscopy of Metal Phthalocyanines: d^7 and d^9 Cases. *J. Am. Chem. Soc.* **1996**, *118*, 7197−7202.

(35) Strohmeier, R.; Ludwig, C.; Petersen, J.; Gompf, B.; Eisenmenger, W. Scanning Tunneling Microscope Investigations of Lead-Phthalocyanine on MoS_2. *J. Vac. Sci. Technol., B* **1996**, *14*, 1079−1082.

(36) Böhringer, M.; Berndt, R.; Schneider, W.-D. Transition from Three-Dimensional to Two-Dimensional Faceting of Ag(110) Induced by Cu-Phthalocyanine. *Phys. Rev. B* **1997**, *55*, 1384−1387.

(37) Lu, X.; Hipps, K. W. Scanning Tunneling Microscopy of Metal Phthalocyanines: d^6 and d^8 Cases. *J. Phys. Chem. B* **1997**, *101*, 5391−5396.

(38) Lackinger, M.; Hietschold, M. Determining Adsorption Geometry of Individual Tin-Phthalocyanine Molecules on Ag(111) - A STM Study at Submonolayer Coverage. *Surf. Sci.* **2002**, *520*, L619−L624.

(39) Papageorgiou, N.; Salomon, E.; Angot, T.; Layet, J.-M.; Giovanelli, L.; Lay, G. L. Physics of Ultra-Thin Phthalocyanine Films on Semiconductors. *Prog. Surf. Sci.* **2004**, *77*, 139−170.

(40) Kröger, J.; Jensen, H.; Néel, N.; Berndt, R. Self-Organization of Cobalt-Phthalocyanine on a Vicinal Gold Surface revealed by Scanning Tunnelling Microscopy. *Surf. Sci.* **2007**, *601*, 4180−4184.

(41) Sperl, A.; Kröger, J.; Berndt, R. Controlled Metalation of a Single Adsorbed Phthalocyanine. *Angew. Chem., Int. Ed.* **2011**, *50*, 5294−5297.

(42) Sperl, A.; Kröger, J.; Berndt, R. Demetalation of a Single Organometallic Complex. *J. Am. Chem. Soc.* **2011**, *133*, 11007−11009.

(43) Sperl, A.; Kröger, J.; Berndt, R. Electronic Superstructure of Lead Phthalocyanine on Lead Islands. *J. Phys. Chem. A* **2011**, *115*, 6973−6978.

(44) Gopakumar, T. G.; Brumme, T.; Kröger, J.; Toher, C.; Cuniberti, G.; Berndt, R. Coverage-Driven Electronic Decoupling of Fe-Phthalocyanine from a Ag(111) Substrate. *J. Phys. Chem. C* **2011**, *115*, 12173−12179.

(45) Kresse, G.; Hafner, J. Ab initio Molecular Dynamics for Liquid Metals. *Phys. Rev. B* **1993**, *47*, 558(R)−561(R).

(46) Kresse, G.; Hafner, J. Ab initio Molecular-Dynamics Simulation of the Liquid-Metal-Amorphous-Semiconductor Transition in Germanium. *Phys. Rev. B* **1994**, *49*, 14251−14269.

(47) Kresse, G.; Furthmüller, J. Efficiency of ab-initio Total Energy Calculations for Metals and Semiconductors Using a Plane-Wave Basis Set. *Comput. Mater. Sci.* **1996**, *6*, 15−50.

(48) Kresse, G.; Furthmüller, J. Efficient Iterative Schemes for ab Initio Total-Energy Calculations using a Plane-Wave Basis Set. *Phys. Rev. B* **1996**, *54*, 11169−11186.

(49) Perdew, J.; Burke, K.; Ernzerhof, M. Generalized Gradient Approximation Made Simple. *Phys. Rev. Lett.* **1996**, *77*, 3865−3868.

(50) Kresse, G.; Joubert, D. From Ultrasoft Pseudopotentials to the Projector Augmented-Wave Method. *Phys. Rev. B* **1999**, *59*, 1758−1775.

(51) Stadler, C.; Hansen, S.; Pollinger, F.; Kumpf, C.; Umbach, E.; Lee, T.-L.; Zegenhagen, J. Structural Investigation of the Adsorption of SnPc on Ag(111) Using Normal-Incidence X-Ray Standing Waves. *Phys. Rev. B* **2006**, *74*, 035404.

(52) Woolley, R. A. J.; Martin, C.; Miller, G.; Dhanak, V.; Moriarty, P. J. Adsorbed Molecular Shuttlecocks: An NIXSW Study of Sn Phthalocyanine on Ag(111) Using Auger Electron Detection. *Surf. Sci.* **2007**, *601*, 1231−1238.

(53) Baran, J. D.; Larsson, J. A.; Woolley, R. A. J.; Cong, Y.; Moriarty, P. J.; Cafolla, A. A.; Schulte, K.; Dhanak, V. R. Theoretical and Experimental Comparison of SnPc, PbPc, and CoPc Adsorption on Ag(111). *Phys. Rev. B* **2010**, *81*, 075413.

(54) Tersoff, J.; Hamann, D. R. Theory and Application for the Scanning Tunneling Microscope. *Phys. Rev. Lett.* **1983**, *50*, 1998−2001.

(55) Tersoff, J.; Hamann, D. R. Theory of the Scanning Tunneling Microscope. *Phys. Rev. B* **1985**, *31*, 805−813.

(56) Hofer, W. A.; Redinger, J. Scanning Tunneling Microscopy of Binary Alloys: First Principles Calculation of the Current for PtX (100) Surfaces. *Surf. Sci.* **2000**, *447*, 51−61.

(57) Hofer, W. A.; Fisher, A. J. Simulation of Spin-Resolved Scanning Tunneling Microscopy: Influence of the Magnetization of Surface and Tip. *J. Magn. Magn. Mater.* **2003**, *267*, 139−151.

(58) Palotás, K.; Hofer, W. A. Multiple Scattering in a Vacuum Barrier Obtained from Real-Space Wavefunctions. *J. Phys.: Condens. Matter* **2005**, *17*, 2705−2713.

(59) The energetically favored adsorption site of a single SnPc on Ag(111) was identified as a bridge site.[31] The different adsorption site for individual SnPc molecules embedded in a closed layer on Ag(111) may be rationalized in terms of additional interactions between adjacent molecules, which change the energy landscape for adsorption sites.

(60) We have estimated a voltage drop across the molecule and the buffer layer of 3−6%. Modeling the tunneling junction as a plate capacitor[10] leads to a voltage drop of $\Delta V = V/\alpha$ with V the applied voltage and $\alpha = \varepsilon z/d + 1$ (ε = dielectric constant, z = tip−molecule distance, d = molecule−surface distance). ε may take values between 10 and 20,[69] $d \approx 0.64$ nm,[51] and z has been estimated as 1 nm.

(61) The experimental LUMO energies of SnPc↑ and SnPc↓ differ by 0.04 eV, which may be due to different adsorption heights of Sn in SnPc↑ and SnPc↓. For FePc on Ag(111) a similar energy shift of a molecular orbital was induced by different adsorption heights.[44] Slightly different adsorption geometries may likewise influence the LUMO energies of SnPc↑ and SnPc↓.

(62) For SnPc↓ corrections due to vibration excitations lead to a collapse of the applied lowest-order perturbation approach (eq 2) since the denominator becomes zero.

(63) Dubay, O.; Kresse, G. Accurate Density Functional Calculations for the Phonon Dispersion Relations of Graphite Layer and Carbon Nanotubes. *Phys. Rev. B* **2003**, *67*, 035401.

(64) Lorente, N. Mode Excitation Induced by the Scanning Tunnelling Microscope. *Appl. Phys. A: Mater. Sci. Process.* **2004**, *78*, 799−806.

(65) Teobaldi, G.; Peñalba, M.; Arnau, A.; Lorente, N.; Hofer, W. A. Including the Probe Tip in Theoretical Models of Inelastic Scanning Tunneling Spectroscopy: CO on Cu(100). *Phys. Rev. B* **2007**, *76*, 235407.

(66) Grein, C. H.; Runge, E.; Ehrenreich, H. Phonon-Assisted Transport in Double-Barrier Resonant-Tunneling Structures. *Phys. Rev. B* **1993**, *47*, 12590.

(67) Faber, C.; Janssen, J. L.; Côté, M.; Runge, E.; Blase, X. Electron-Phonon Coupling in the C_{60} Fullerene within the Many-Body GW Approach. *Phys. Rev. B* **2011**, *84*, 155104.

(68) Repp, J.; Liljeroth, P.; Meyer, G. Coherent Electron-Nuclear Coupling in Oligothiophene Molecular Wires. *Nat. Phys.* **2010**, *6*, 975−979.

(69) Ramprasad, R.; Shi, N. Polarizability of Phthalocyanine Based Molecular Systems: A First-Principles Electronic Structure Study. *Appl. Phys. Lett.* **2006**, *88*, 222903.